A Kinetic Model for Industrial Gas-Phase Ethylene Copolymerization

A dynamic kinetic model describing gas-phase olefin copolymerization using a multiple active site Ziegler-Natta catalyst is presented. This model is capable of predicting production rate, molecular weight, and copolymer composition changes observed in an industrial reactor. The model also explains how broad molecular weight distributions and bimodal copolymer compositions can occur as has been observed for commercial linear polyethylenes.

K. B. McAuley
J. F. MacGregor
A. E. Hamielec
Department of Chemical Engineering
McMaster Institute for Polymer Production Technology
McMaster University
Hamilton, Ontario, Canada L8S 4L7

Introduction

Until recently, the cause of broad molecular weight distribution and compositional inhomogeneity observed in steady-state olefin copolymerization with Ziegler-Natta (ZN) catalysts remained poorly understood. Some causes, however, have been proposed including: the existence of more than one type of reactive site on the catalyst surface (Floyd et al., 1988) and the existence of concentration gradients within polymer particles caused by diffusional phenomena (Nagel et al., 1980). If a catalyst surface contains different types of active site structures, each with its own characteristic kinetic rate constants for propagation, copolymerization and transfer reactions, copolymers with broad molecular weight, and compositional distributions can be produced. Alternatively, if diffusional barriers to mass transfer govern the reaction rate, catalyst sites at different radial positions in a growing polymer particle are subject to different reactant concentrations, which can account for a broad distribution of molecular weights and composition (Galvan, 1986).

Authors of recent literature reviews and modeling studies (Zucchini and Cecchin, 1983; deCarvalho et al., 1989; Boehm et al., 1986; Galvan and Tirrell, 1986) have concluded that broad molecular weight distributions produced by heterogeneous ZN catalysts are most likely the result of multiple active sites, although in certain instances (very broad particle size distributions or high molecular weight comonomers) diffusional resistances could play some role. The most convincing evidence cited for the existence of more than one type of active site has been provided by Usami et al. (1986) who have studied linear low-density polyethylene (LLDPE) copolymers of ethylene and butene. They collected LLDPE samples produced by processes with very different monomer mass transfer characteristics, such as solution, slurry, gas phase, and bulk polymerization. All of these samples had been polymerized using titanium (Ti)-based heterogeneous ZN catalysts. Cross-fractionation according to short chain branching (SCB) frequency and molecular weight distribution was performed by temperature rise elution fractionation (TREF) and by size exclusion chromatography (SEC). Usami et al. (1986) found that all of the LLDPE samples had a characteristic bimodal SCB distribution which could not have been caused by diffusional effects. They attributed their experimental findings to the existence of at least two types of active catalyst sites. One site produces butene-rich, low-molecular-weight material, and the other produces a higher-molecular-weight polymer with lower butene incorporation and hence fewer short-chain branches.

In this paper, a dynamic multiple active site model to describe the copolymerization of ethylene and alpha-olefins in a gas-phase fluidized-bed reactor is presented. A schematic diagram of a typical configuration for an industrial reactor system is shown in Figure 1 (Burdett, 1988). The feed to the reactor comprises ethylene, comonomers (1-butene and/or 1-hexene), hydrogen, and nitrogen. These gases provide the fluidization and heat transfer media and supply reactants for the growing polymer particles. A Ti-based heterogeneous ZN catalyst and a triethyl aluminum cocatalyst are fed continuously to the reactor. The fluidized particles disengage from the reactant gas in the expanded top section of the reactor. The unreacted gases are combined with fresh feed streams and recycled to the base of the reactor. Since the reaction is highly exothermic, heat must be removed from the cycle gas before it is returned to the reactor. The conversion per pass through the bed is very low (2–3%). Thus, the recycle stream is much larger than fresh feed streams. Periodically the product discharge valve near the base of the

Correspondence concerning this paper should be addressed to J. F. MacGregor.

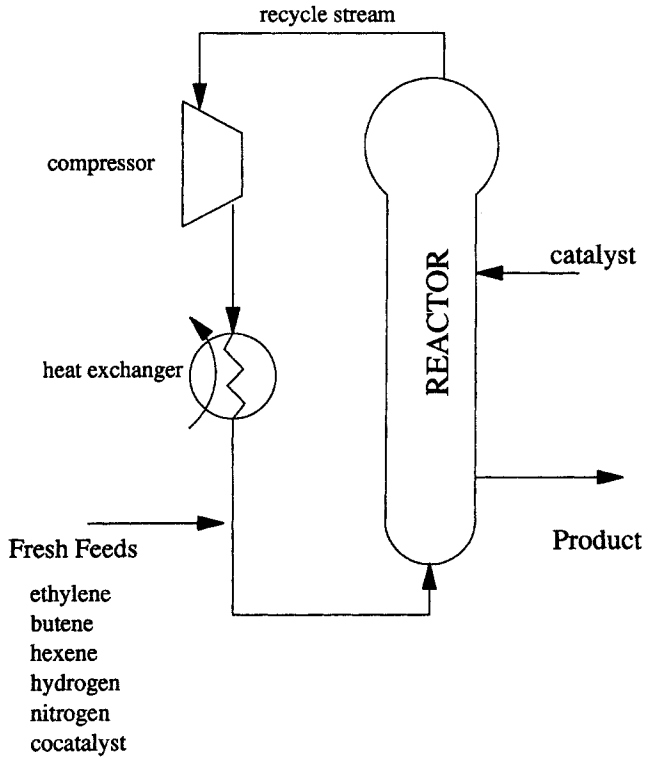

Figure 1. Industrial fluidized-bed polyethylene reactor.

reactor opens and fluidized product flows into a surge tank. The unreacted gas is recovered from the product which proceeds to the finishing area of the plant for additive incorporation and pelletization.

Other authors (Galvan, 1986; Choi and Ray, 1985; Hutchinson and Ray, 1987) have presented models for gas-phase ethylene polymerization in fluidized-bed reactors in order to investigate temperature control problems and to predict system stability. To explain these phenomena, a comprehensive model detailing heat, mass and momentum transfer among the phases of the fluidized bed is required (Kunii and Levenspiel, 1968). The present model, however, has been developed to predict copolymer composition and molecular weight properties in an industrial-scale fluidized-bed reactor under good temperature regulation. Because of the uniform temperature distribution in the bed, the large recycle stream and kinetic rather than diffusion control of the reaction rate, this system can be modeled as a well-mixed gas in equilibrium with a solid phase. As such, the main modeling effort has been focused on characterizing the copolymerization kinetics occurring at the multiple active sites of the catalyst. Two potential uses for such a model are the simulation and testing of on-line quality control schemes and the prediction of the effects of grade transition policies on molecular weight and compositional distributions.

Reaction Mechanisms

The mechanisms described here are similar to those outlined by Kissin (1987) and deCarvalho et al. (1989). In general, each site type is associated with different rate constants for formation, initiation, propagation, and transfer. These reaction mechanisms consider the effects of terminal monomers on reaction rates; penultimate effects are neglected. The model is developed to account for any number of active site types and for copolymerization of ethylene and several comonomers. Throughout this section, the index j will refer to the type of active site and i will refer to the monomer type.

Formation and initiation of active sites

Potential active sites of type j undergo a formation reaction with the organometallic cocatalyst (Kissin, 1987). If the cocatalyst concentration is constant and in excess, this reaction can be described as:

$$N^*(j) \xrightarrow{kf(j)} N(0,j) \tag{1}$$

where $kf(j)$ is a pseudorate constant for the formation reaction, $N^*(j)$ is a potential active site of type j, and $N(0,j)$ is an active site of type j with no attached monomer.

The newly formed sites undergo initiation reactions with monomers:

$$N(0,j) + M_i \xrightarrow{ki_i(j)} N_i(1,j) \quad i = 1, 2 \ldots \tag{2}$$

M_i denotes monomer of type i. If $i = 1$, the monomer is ethylene; $i = 2$ and $i = 3$ correspond to alpha-olefin comonomers such as butene or hexene. $ki_i(j)$ is an initiation rate constant and $N_i(1,j)$ is a living polymer chain of length one.

Propagation

Living polymer chains grow by the following propagation reactions:

$$N_i(r,j) + M_k \xrightarrow{kp_{ik}(j)} N_k(r+1,j)$$

$$i = 1, 2, \ldots \quad k = 1, 2, \ldots \tag{3}$$

$N_i(r,j)$ is a living polymer chain of length r with terminal monomer i attached to the active center of type j. $kp_{ik}(j)$ is the propagation rate constant for the reaction of monomer M_k with an active center of type j, bonded to a terminal monomer M_i.

Chain transfer reactions

Most dead polymer chains are produced by chain transfer reactions. These reactions occur with monomers, hydrogen, and organometallic cocatalyst. As well, spontaneous transfer reactions have been documented (Kissin, 1987).

Transfer to Monomer. The following chain transfer to monomer reactions can occur:

$$N_i(r,j) + M_k \xrightarrow{kfm_{ik}(j)} N_k(1,j) + Q(r,j)$$

$$i = 1, 2, \ldots \quad k = 1, 2, \ldots \tag{4}$$

$Q(r,j)$ is a dead polymer segment of length r which cannot undergo any further reactions. Note that transfer to monomer reactions produce living polymer chains of length one, $N_k(1,j)$, which can propagate to form new polymer chains.

Transfer to Hydrogen. Hydrogen is added to industrial reactors making linear polyethylene to control molecular weight

development via chain transfer:

$$N_i(r,j) + H_2 \xrightarrow{kfh_i(j)} N_H(0,j) + Q(r,j) \qquad i = 1, 2, \ldots \quad (5)$$

Species $N_H(0,j)$ is an active site with no reacted monomer which can undergo reinitiation reactions:

$$N_H(0,j) + M_i \xrightarrow{kh_i(j)} N_i(1,j) \quad i = 1, 2, \ldots \quad (6)$$

These sites are quickly reinitiated by reactions with the cocatalyst. If the cocatalyst is triethyl aluminum, $AlEt_3$, the reinitiation reaction is (Kissin, 1987):

$$N_H(0,j) + AlEt_3 \xrightarrow{kh_r(j)} N_1(1,j) \quad (7)$$

The product $N_1(1,j)$ has the same reactive characteristics as the sites produced by initiation and transfer reactions with ethylene. This is not the case for a general cocatalyst.

Transfer to Cocatalyst. Growing polymer chains can undergo transfer reactions with the cocatalyst:

$$N_i(r,j) + AlEt_3 \xrightarrow{kfr_i(j)} N_1(1,j) + Q(r,j) \qquad i = 1, 2, \ldots \quad (8)$$

Spontaneous Transfer. Depending on the catalyst, spontaneous transfer reactions may be significant for some or all site types:

$$N_i(r,j) \xrightarrow{kfs_i(j)} N_H(0,j) + Q(r,j) \quad i = 1, 2, \ldots \quad (9)$$

The sites produced by spontaneous transfer are thought to have a structure similar to those produced by transfer to hydrogen reactions (Kissin, 1987).

Deactivation reactions

Active sites may decay spontaneously to form dead sites and dead polymer chains:

$$N_i(r,j) \xrightarrow{kds(j)} N_d(j) + Q(r,j) \quad i = 1, 2, \ldots \quad (10)$$

$$N(0,j) \xrightarrow{kds(j)} N_d(j) \quad (11)$$

$$N_H(0,j) \xrightarrow{kds(j)} N_d(j) \quad (12)$$

where $N_d(j)$ is a dead site of type j and $kds(j)$ is a decomposition rate constant. In this formulation, it has been assumed that the rate of deactivation is not influenced by the terminal monomer nor chain length.

Reactions with poisons

Even low levels of some reactive impurities, such as carbon monoxide, can cause a nearly instantaneous drop in propagation rates. The adsorption of such an impurity onto a catalyst site renders it inactive:

$$N_i(r,j) + I_m \xrightarrow{kdI(j)} N_{dIH}(0,j) + Q(r,j) \qquad i = 1, 2, \ldots \quad (13)$$

$$N_H(0,j) + I_m \xrightarrow{kdI(j)} N_{dIH}(0,j) \quad (14)$$

$$N(0,j) + I_m \xrightarrow{kdI(j)} N_{dI}(0,j) \quad (15)$$

I_m is the impurity, $kdI(j)$ is an impurity deactivation rate constant, and $N_{dIH}(0,j)$ and $N_{dI}(0,j)$ are sites deactivated by adsorbed impurities. The reactions above may be reversible for some poisons, in which case, desorption of the impurity leaves sites that can undergo reinitiation reactions:

$$N_{dIH}(0,j) \xrightarrow{ka(j)} N_H(0,j) + I_m \quad (16)$$

$$N_{dI}(0,j) \xrightarrow{ka(j)} N(0,j) + I_m \quad (17)$$

$ka(j)$ is an impurity desorption rate constant.

Model Development

When modeling a single-pass fluidized-bed reactor or a recycle reactor with high conversion per pass, one must account for gas-phase concentration gradients between the bottom and top of the bed and for mass transfer between bubble and emulsion phases. However, the modeling of the input/output characteristics of a recycle-dominated fluidized-bed reactor for polymers can be simplified greatly by making suitable assumptions. Since the industrial fluidized-bed reactor system under consideration has a sizable recycle stream and a low conversion per pass through the bed, the vertical concentration gradient through the bed is very small and can be neglected. Backmixing of both the gas and solid phases in the fluidized bed does occur. However, even if the gas experienced pure plug flow through the fluidized bed, the large recycle to fresh feed ratio would make the well-mixed assumption valid for the gas phase since recycle plug-flow reactor dynamics approach those of continuous stirred-tank reactors (CSTR) as the recycle to fresh feed ratio becomes very large (Levenspiel, 1972). In normal industrial reactor operation, the recycle to fresh feed ratio is approximately 40:1. Thus modeling the fluidized-bed reactor plus recycle system as a CSTR containing a well-mixed solid phase interacting with a well-mixed gas phase is justified.

Thermocouples at different vertical positions in the reactor indicate that vertical temperature gradients are small in the reaction zone. A rise of less than 3°C between the gas distributor plate, located below the reaction zone, and the top of the bed is typical. In this model it is assumed that the effects of any small radial or vertical temperature gradients can be neglected.

Gas-phase concentrations vs. concentrations of species at active sites

When new catalyst particles are injected into a gas-phase reactor, the active sites are quickly covered by the growing polymer chains. Thus, reaction rates are controlled by the concentrations of reactants dissolved in the polymer surrounding the sites rather than by bulk concentrations in the gas phase. In general, the solubility of gaseous substances in olefin polymers depends on the degree of crystallinity. Gases are sorbed only into the amorphous regions of the polymer. In a recent paper, Hutchinson and Ray (1988) suggest that, during the reaction, successive polymerization and crystallization occur. Since the polymer chains grow away from the catalyst surface, the polymer at the sites is in a nascent, amorphous state. Thus, the crystallinity or density of the polymer being produced is not expected to affect monomer concentrations at the catalyst sites.

Since diffusional resistances can usually be neglected (Floyd et al., 1986), the concentrations of species at the active sites are assumed to be the equilibrium concentrations in the amorphous polymer. Hutchinson and Ray (1988) conclude that single-component hydrogen and ethylene sorption in amorphous polyethylene, at the pressures encountered in the gas-phase reactor, can be satisfactorily modeled by Henry's law. However, more soluble, heavier monomers such as butene and hexene are predicted to exhibit solubilities at least 5% greater than those predicted by Henry's law. Swelling of the amorphous polymer by the heavier sorbed butene and hexene results in a somewhat enhanced solubility of ethylene, hydrogen, and heavy components, alike, giving rise to higher reaction rates than would occur in the unswollen polymer. No systematic study has been done to examine and quantify these effects.

To develop a model which can predict polymer quality variables and reaction rate from gas-phase concentrations, the following assumptions are made. First, it is assumed that the amorphous polymer phase is in equilibrium with the gas phase and that diffusional effects within the amorphous phase are negligible. Secondly, the plasticizing effects of dissolved monomers on solubilities in the polymer are neglected. When multicomponent relationships become available to predict solubilities in amorphous polyethylene, this information can easily be incorporated into the model. These assumptions lead to the conclusion that the partition coefficients for individual components between the gas and polymer phases remain constant. For each component one can write:

$$[M_i]_{\text{pol}} = K_p[M_i]_{\text{gas}} \tag{18}$$

where $[M_i]_{\text{pol}}$ and $[M_i]_{\text{gas}}$ are the concentrations of component i at the catalyst sites within the polymer particles and in the gas phase, respectively. K_p is a partition coefficient. If the rate, R, of a certain reaction, occurring at a site of type j is given by,

$$R = k[M_i]_{\text{pol}}Y(0,j) \tag{19}$$

where k is a rate constant and $Y(0,j)$ is the number of moles of active sites of type j in the reactor, then one can also write:

$$R = k^*[M_i]_{\text{gas}}Y(0,j) \tag{20}$$

where

$$k^* = (kK_p) \tag{21}$$

is a pseudorate constant. In the following model equations, all rate constants are of the same type as k^*, and all concentrations are those in the gas phase. This convention is used because gas-phase concentrations are measured on-line in the industrial reactor, whereas concentrations in the amorphous polymer are not well known.

Mass balance equations for active sites

Mass balances of the form:

$$\text{Accumulation} = \text{Inflow} + \text{Generation} - \text{Consumption} - \text{Outflow} \tag{22}$$

can be developed for each reacting species. The balance on the number of moles of potential active sites $N^*(j)$ in the reactor is given by:

$$\frac{dN^*(j)}{dt} = F^*_{in}(j) - kf(j)N^*(j) - N^*(j)\frac{R_v}{V_p} \tag{23}$$

where $F^*_{in}(j)$ is the molar flow rate of potential active sites into the reactor which is proportional to the mass feed rate of the catalyst, R_v is the volumetric flow rate of polymer from the reactor and V_p is the volume of the polymer phase in the reactor. Similarly, for the number of moles of initiation sites $N(0,j)$ and $N_{\text{H}}(0,j)$:

$$\frac{dN(0,j)}{dt} = kf(j)N^*(j) + ka(j)N_{dI}(0,j) - N(0,j) \cdot \left\{ki_T(j)[M_T] + kds(j) + kdI(j)[I_m] + \frac{R_v}{V_p}\right\} \tag{24}$$

$$\frac{dN_{\text{H}}(0,j)}{dt} = Y(0,j)\{kfh_T(j)[\text{H}_2] + kfs_T(j)\} + ka(j)\,N_{dI\text{H}}(0,j) - N_{\text{H}}(0,j)\left\{kh_T(j)[M_T] + kds(j) + kh_r(j)[\text{AlEt}_3] + kdI(j)[I_m] + \frac{R_v}{V_p}\right\} \tag{25}$$

where $[M_T]$ is the total molar monomer concentration given by:

$$[M_T] = [M_1] + [M_2] + \ldots \tag{26}$$

$[M_1]$, $[M_2]$, $[M_3]$ and $[\text{H}_2]$ are the concentrations of ethylene, butene, hexene, and hydrogen, respectively. $Y(0,j)$ is the zeroth moment of the living polymer chain length distribution:

$$Y(0,j) = \sum_{r=1}^{\infty}\{N_1(r,j) + N_2(r,j) + \ldots\} \tag{27}$$

$ki_T(j)$, $kfh_T(j)$, $kfs_T(j)$, and $kh_T(j)$ are pseudokinetic rate constants.

The following mass balance can be written for initiated polymer chains of length one with ethylene as the terminal monomer:

$$\frac{dN_1(1,j)}{dt} = ki_1(j)N(0,j)[M_1] + N_H(0,j)\{kh_1(j)[M_1] + kh_r(j)[AlEt_3]\} + Y(0,j)\{kfm_{T1}(j)[M_1] + kfr_T(j)[AlEt_3]\} - N_1(1,j)\left\{kp_{1T}(j)[M_T] + kfm_{1T}(j)[M_T] + kfh_1(j)[H_2] + kfr_1(j)[AlEt_3] + kfs_1(j) + kds(j) + kdI(j)[I_m] + \frac{R_v}{V_p}\right\} \quad (28)$$

Similarly, for any other terminal monomer, M_i:

$$\frac{dN_i(1,j)}{dt} = ki_i(j)N(0,j)[M_i] + N_H(0,j)kh_i(j)[M_i] + Y(0,j)kfm_{Ti}(j)[M_i] - N_i(1,j)\left\{kp_{iT}(j)[M_T] + kfm_{iT}(j)[M_T] + kfh_i(j)[H_2] + kfr_i(j)[AlEt_3] + kfs_i(j) + kds(j) + kdI(j)[I_m] + \frac{R_v}{V_p}\right\} \quad i = 2, 3, \ldots \quad (29)$$

The number of moles of impurity deactivated sites conform to the following mass balances:

$$\frac{dN_{dlH}(0,j)}{dt} = kdI(j)[I_m]\{Y(0,j) + N_H(0,j)\} - N_{dlH}(0,j)\left\{ka(j) + \frac{R_v}{V_p}\right\} \quad (30)$$

$$\frac{dN_{dl}(0,j)}{dt} = kdI(j)[I_m]N(0,j) - N_{dl}(0,j)\left\{ka(j) + \frac{R_v}{V_p}\right\} \quad (31)$$

Balances on living polymer of chain length r with terminal monomers M_i ($i = 1, 2, \ldots$) were generated and added together to give the following mass balance on $Y(0,j)$, the zeroth moment of the living polymer chain length distribution:

$$\frac{dY(0,j)}{dt} = [M_T]\{ki_T(j)N(0,j) + kh_T(j)N_H(0,j)\} + kh_r(j)N_H(0,j)[AlEt_3] - Y(0,j)\left\{kfh_T(j)[H_2] + kfs_T(j) + kds(j) + kdI(j)[I_m] + \frac{R_v}{V_p}\right\} \quad (32)$$

Mass balances on the first and second moments of the living polymer distribution were determined as well:

$$\frac{dY(1,j)}{dt} = [M_T]\{ki_T(j)N(0,j) + kh_T(j)N_H(0,j)\} + kh_r(j)N_H(0,j)[AlEt_3] + [M_T]kp_{TT}(j)Y(0,j) + \{Y(0,j) - Y(1,j)\}\{kfm_{TT}(j)[M_T] + kfr_T(j)[AlEt_3]\} - Y(1,j)\left\{kfh_T(j)[H_2] + kfs_T(j) + kds(j) + kdI(j)[I_m] + \frac{R_v}{V}\right\} \quad (33)$$

$$\frac{dY(2,j)}{dt} = [M_T]\{ki_T(j)N(0,j) + kh_T(j)N_H(0,j)\} + kh_r(j)N_H(0,j)[AlEt_3] + [M_T]kp_{TT}(j)\{2Y(1,j) - Y(0,j)\} + \{Y(0,j) - Y(2,j)\}\{kfm_{TT}(j)[M_T] + kfr_T(j)[AlEt_3]\} - Y(2,j)\left\{kfh_T(j)[H_2] + kfs_T(j) + kds(j) + kdI(j)[I_m] + \frac{R_v}{V_p}\right\} \quad (34)$$

where $Y(n,j)$ the nth moment of the living polymer chain length distribution, is given by:

$$Y(n,j) = \sum_{r=1}^{\infty} r^n\{N_1(r,j) + N_2(r,j) + \ldots\} \quad n = 0, 1, 2 \ldots \quad (35)$$

The molecular weight of the polymer produced in the reactor is determined by the method of moments. As such, the following balances are required for the nth moments of the chain length distributions for dead polymer chains:

$$\frac{dX(n,j)}{dt} = \{Y(n,j) - N_T(1,j)\}\{kfm_{TT}(j)[M_T] + kfr_T(j)[AlEt_3] + kfh_T(j)[H_2] + kfs_T(j) + kds(j) + kdI(j)[I_m]\} - X(n,j)\frac{R_v}{V_p} \quad n = 0, 1, 2 \quad (36)$$

The moments of the dead polymer distribution are defined by:

$$X(n,j) = \sum_{r=2}^{\infty} r^n Q(r,j) \quad (37)$$

The summation above starts at $r = 2$ because dead chains of length 1 are not considered polymer. The mass balances for the moments of the dead polymer chain length distribution were obtained by writing a mass balance on dead polymer segments of

length r and substituting the result into the definition for the moments given above.

Pseudokinetic rate constants

The use of pseudokinetic rate constants for general copolymerization kinetics is outlined by Hamielec et al. (1987). The model mass balance equations contain the following pseudokinetic rate constants which depend upon the composition of the reaction medium and upon the distribution of terminal monomers at each site type. The pseudokinetic rate constants shown here are for a three-monomer system. The definitions can be expanded to include more monomer types if required.

Pseudorate constant $kh_T(j)$ is defined as:

$$kh_T(j) = f_1 kh_1(j) + f_2 kh_2(j) + f_3 kh_3(j) \tag{38}$$

An analogous relationship can be written for $ki_T(j)$. f_i is the mole fraction of the total monomer which is of type i:

$$f_i = \frac{[M_i]}{[M_1] + [M_2] + [M_3]} \tag{39}$$

There are three types of pseudokinetic propagation constants used in the model:

$$kp_{iT}(j) = f_1 kp_{i1}(j) + f_2 kp_{i2}(j) + f_3 kp_{i3}(j) \tag{40}$$

$$kp_{Ti}(j) = \phi_1(j) kp_{1i}(j) + \phi_2(j) kp_{2i}(j) + \phi_3(j) kp_{3i}(j) \tag{41}$$

$$kp_{TT}(j) = f_1 kp_{T1}(j) + f_2 kp_{T2}(j) + f_3 kp_{T3}(j) \tag{42}$$

$\phi_i(j)$ is the fraction of active sites of type j having terminal monomer M_i. For a three-monomer system:

$$\phi_1(j) = \frac{f_1^2 kp_{21}(j) kp_{31}(j) + f_1 f_2 kp_{21}(j) kp_{32}(j) + f_1 f_3 kp_{23}(j) kp_{31}(j)}{\Psi(j)} \tag{43}$$

$$\phi_2(j) = \frac{f_1 f_2 kp_{12}(j) kp_{31}(j) + f_2^2 kp_{12}(j) kp_{32}(j) + f_2 f_3 kp_{13}(j) kp_{32}(j)}{\Psi(j)} \tag{44}$$

$$\phi_3(j) = 1 - \phi_1(j) - \phi_2(j) \tag{45}$$

where the denominator $\Psi(j)$ is given by:

$$\begin{aligned}\Psi(j) = {} & f_1^2 kp_{21}(j) kp_{31}(j) + f_1 f_2 kp_{21}(j) kp_{32}(j) \\ & + f_1 f_3 kp_{23}(j) kp_{31}(j) \\ & + f_1 f_2 kp_{12}(j) kp_{31}(j) + f_2^2 kp_{12}(j) kp_{32}(j) \\ & + f_2 f_3 kp_{13}(j) kp_{32}(j) \\ & + f_2 f_3 kp_{12}(j) kp_{23}(j) + f_1 f_3 kp_{13}(j) kp_{21}(j) \\ & + f_3^2 kp_{13}(j) kp_{23}(j)\end{aligned} \tag{46}$$

The equations for $\phi_i(j)$ were obtained by making the second long chain approximation for growing polymer chains.

The transfer to monomer pseudorate constants $kfm_{iT}(j)$, $kfm_{Ti}(j)$, and $kfm_{TT}(j)$ are defined analogously to the propagation pseudorate constants. The three other transfer pseudorate constants for transfer to hydrogen, to cocatalyst and for spontaneous transfer are:

$$kfh_T(j) = \phi_1(j) kfh_1(j) + \phi_2(j) kfh_2(j) + \phi_3(j) kfh_3(j) \tag{47}$$

$$kfr_T(j) = \phi_1(j) kfr_1(j) + \phi_2(j) kfr_2(j) + \phi_3(j) kfr_3(j) \tag{48}$$

$$kfs_T(j) = \phi_1(j) kfs_1(j) + \phi_2(j) kfs_2(j) + \phi_3(j) kfs_3(j) \tag{49}$$

Mass balances for reacted monomers in the copolymer

In order to predict the composition of the copolymer in the reactor at any time, mass balances have been performed on the number of moles of each type of monomer incorporated or bound in the polymer particles:

$$\frac{dB_i}{dt} = R_i - B_i \frac{R_v}{V_p} \quad i = 1, 2, \ldots \tag{50}$$

B_i is the number of moles of monomer i which are bound in the polymer in the reactor and R_i is the instantaneous consumption rate of monomer i to form polymer. Assuming that the only significant consumption of monomers is by propagation gives the following expression for consumption rate:

$$R_i = \sum_{j=1}^{NS} [M_i]\, Y(0, j)\, kp_{Ti}(j) \quad i = 1, 2, \ldots \tag{51}$$

where NS is the number of types of active sites. The volumetric outflow rate of polymer, R_v, which appears in the model equations can be determined from the consumption rates of the monomers and from the rate of change of the weight of polymer in the reactor:

$$R_v = \frac{mw_1 R_1 + mw_2 R_2 + \ldots}{\rho} - \frac{dB_w/dt}{\rho} \tag{52}$$

mw_i is the molecular weight of monomer i in g/mol, ρ is the density of the polymer in g/L, and B_w is the mass of resin in the reactor.

Model simplication

The set of model equations has been solved numerically by LSODE, a differential equation solving package (Hindmarsh, 1980). This set of equations is stiff because the dynamics associated with changes in intermediate species $N^*(j)$, $N_H(0, j)$, $N(0, j)$ and $N_i(1, j)$ are very fast compared to the dynamics associated with the other states in the model. In order to reduce the computational effort for model solution, the stationary state hypothesis was made for these species. The corresponding differential equations were, thus, converted to algebraic equations by setting the lefthand-side derivative terms to zero. Simulations were performed, using realistic rate constants, to

compare the predictions of the full set of stiff equations with those of the nonstiff system of algebraic and differential equations solved in the simplified model. No significant differences between the two solutions were observed, indicating that the pseudosteady-state hypothesis was valid.

Copolymer composition and molecular weight properties

The mole fraction of each reacted comonomer bound in the polymer, F_i, can be calculated from:

$$F_i = \frac{B_i}{B_1 + B_2 + \ldots} \quad i = 1, 2, \ldots \tag{53}$$

The cumulative number and weight average molecular weights, $\overline{M}_n$ and $\overline{M}_w$, can be determined using the method of moments:

$$\overline{M}_n = \frac{\overline{m} \sum_{j=1}^{NS} \{X(1,j) + Y(1,j)\}}{\sum_{j=1}^{NS} \{X(0,j) + Y(0,j)\}} \tag{54}$$

$$\overline{M}_w = \frac{\overline{m} \sum_{j=1}^{NS} \{X(2,j) + Y(2,j)\}}{\sum_{j=1}^{NS} \{X(1,j) + Y(1,j)\}} \tag{55}$$

where $\overline{m}$ is the mean monomer molecular weight defined by:

$$\overline{m} = mw_1 F_1 + mw_2 F_2 + \ldots \tag{56}$$

The polydispersity, Z, is defined by the ratio of weight average to number average molecular weights:

$$Z = \frac{\overline{M}_w}{\overline{M}_n} \tag{57}$$

Note that although this model predicts that each active site type produces polymer with a polydispersity of 2, the cumulative polymer produced at all sites can have a much broader molecular weight distribution (Floyd et al., 1988).

In addition to cumulative average molecular weights and copolymer compositions, the entire instantaneous molecular weight and compositional distributions can be generated for polymer produced at each site type using the Stockmayer (1945) bivariate distribution for two monomer systems. In Ziegler-Natta systems, the only important reactions which produce dead polymer chains are transfer reactions. Thus, the Stockmayer (1945) equation for the weight fraction of dead polymer produced at a site of type j which has chain length between r and $r + dr$ and composition between y and $y + dy$ can be expressed as:

$$W(r,y,j)drdy = \tau(j)^2 r \exp(-\tau(j)r)dr \frac{1}{\sqrt{2\pi\sigma(j)^2}} \exp\left(\frac{-y^2}{2\sigma(j)^2}\right)dy \tag{58}$$

$\tau(j)$ is the ratio of the total rate of chain transfer to the total rate of propagation at the sites of type j:

$$\tau(j) = \frac{kfm_{TT}(j)[M_T] + kfh_T(j)[H_2] + kfr_T(j)[AlEt_3] + kfs_T(j)}{kp_{TT}(j)[M_T]} \tag{59}$$

$\sigma(j)^2$ is the variance of the compositional distribution at the sites of type j given by:

$$\sigma(j)^2 = \overline{F_1}(j)(1 - \overline{F_1})\kappa/r \tag{60}$$

$$\kappa = \{1 + 4\overline{F_1}(j)[1 - \overline{F_1}(j)](r_1 r_2 - 1)\}^{0.5} \tag{61}$$

y is the deviation of the composition from $\overline{F}_1(j)$, the mean mole fraction of ethylene in the dead polymer chains produced instantaneously at sites of type j:

$$\overline{F_1}(j) = \frac{R_1(j)}{R_1(j) + R_2(j)} \tag{62}$$

where $R_i(j)$ is the instantaneous rate of consumption of monomer i at sites of type j:

$$R_i(j) = kp_{Ti}[M_i]Y(0,j) \tag{63}$$

The individual site-specific distributions can then be combined to give the overall instantaneous composition and chain length distribution:

$$W(r,y)drdy = \frac{\sum_{j=1}^{NS} M_x(j)W(r,y,j)drdy}{\sum_{j=1}^{NS} \int_y \int_r M_x(j)W(r,y,j)drdy} \tag{64}$$

$M_x(j)$ is the instantaneous mass rate of production of polymer at sites of type j:

$$M_x(j) = mw_1 R_1(j) + mw_2 R_2(j) + \ldots \tag{65}$$

The overall compositional distribution is obtained by integrating the expression for $W(r,y)drdy$ over all chain lengths. Similarly, $W(r,y)drdy$ can be integrated over all compositions to obtain the molecular weight distribution.

In the original development of the Stockmayer (1945) equation, it was assumed that the molecular weights of the two monomers were equal. For cases when the monomers have molecular weights which differ by an order of magnitude, a correction factor developed by Tacx et al. (1988) can be used to account for the effect of the monomer molecular weight difference. For the ethylene/butene copolymers considered in this study, the frequency distributions predicted by the corrected and uncorrected Stockmayer distribution differed by less than 2%, even at the site characterized by high butene incorporation. Thus, the simpler uncorrected Stockmayer distribution was used for instantaneous molecular weight and compositional distributions.

Melt index and density predictions

The model solution predicts reaction rate, weight and number average molecular weights and comonomer composition from reactor operating conditions. In the industrial reactor, the reaction rate is estimated on-line using an energy balance. Fundamental molecular weight and compositional properties, however, are neither measured on-line nor in the quality control laboratory. Instead, melt index (MI) and density which are related to molecular weight and composition are determined. In order to compare model predictions with operating results, it is necessary to relate MI and density to fundamental properties predicted by the model.

Sinclair (1983) has compiled a collection of data from commercial and patent literature. A graph of melt index vs weight average molecular weight, $\overline{M}_w$, has been plotted from data in this report and is shown in Figure 2. From the data, it appears that MI and $\overline{M}_w$ can be related by a power law. Linear regression was performed on the data in Figure 2 to yield the following correlation:

$$\ln(\overline{M}_w) = 11.622 - 0.288 \ln(MI) \tag{66}$$

or

$$\overline{M}_w = 111{,}525\, MI^{-0.288} \tag{67}$$

This equation has been used to convert laboratory MI results to approximate weight average molecular weights for comparison with model predictions. Since melt index is inversely proportional to the apparent viscosity of the molten polymer under low shear, η, the preceding equation can be written as:

$$\overline{M}_w \propto \eta^{0.288} \tag{68}$$

or

$$\eta \propto \overline{M}_w^{3.47} \tag{69}$$

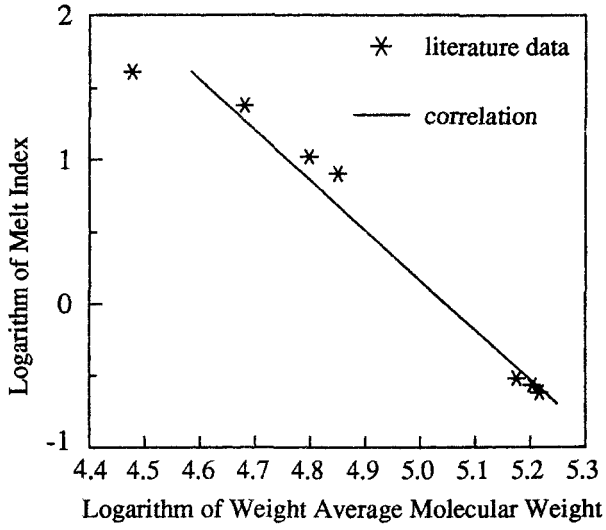

Figure 2. Correlation between molecular weight and melt index.

This relationship corresponds to the general observation (Vinogradov and Malkin, 1980) for linear polymers that:

$$\eta = bM_w^{3.5} \quad M_w \geq M_c \tag{70}$$

where M_w is the molecular weight of the monodisperse polymer fraction and M_c is the critical molecular weight above which this expression is valid. The critical molecular weight for polyethylene is approximately 4,000. The preceding power law equation is valid for polydisperse polymers where M_w is the weight average molecular weight, provided that the fraction of the polymer with molecular weight less than M_c insignificant. This is the case for the polyethylenes produced in the industrial reactor.

The relationship between density and polymer structure is complex. Density is influenced by both the number and length of the short chain branches (Sinclair, 1980) and to a small extent by the polymer molecular weight. An empirical correlation has been developed to relate the density of linear polyethylene to comonomer incorporation in the polymer:

$$\rho = 0.966 - AC_x^B \tag{71}$$

C_x is the mole percent of the comonomer in the polymer and A and B are comonomer-dependent parameters. The model structure was chosen so that the density of the polymer approaches the density of ethylene homopolymer, 0.966 g/mL, as the comonomer content approaches zero. For butene grades, A and B have been fitted at 0.02386 and 0.514. A plot of the correlation and the commercial and patent data from Sinclair (1980) which was used for parameter estimation is given in Figure 3. This relationship was used to convert laboratory density measurements to comonomer incorporation data so that reactor operating data and model predictions could be compared quantitatively.

Model Validation

Two interesting historical data sets from the industrial process were chosen for model validation. During the correspond-

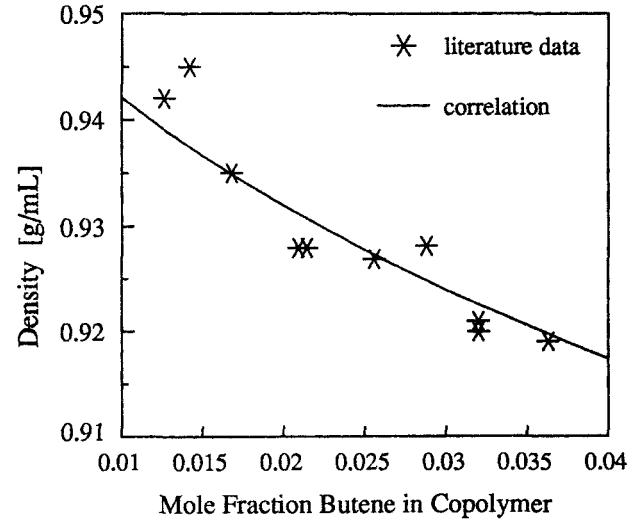

Figure 3. Correlation between composition and density.

ing operating periods, the reactor temperature remained constant and 1-butene was used as the comonomer. Input data to the computer model included the measured reactant gas concentrations, reactor pressure, catalyst and cocatalyst feed rates, and the mass of polymer in the fluidized bed.

Choosing rate constants

Experimental determination of rate constants for multiple site systems is not a trivial task. deCarvalho et al. (1989) discuss one methodology which involves cross-fractionation of polymer samples by TREF and SEC followed by ^{13}C NMR analysis of the cross-fractions (Wild et al., 1982; Usami et al., 1986). In this manner the polymer sample can be divided into fractions produced at individual site types. Important rate parameters can then be determined from the NMR results and reactor operating conditions. To obtain parameter estimates using this technique would require an experimental design wherein the reactor operated under many sets of conditions. Once the experimental measurements were obtained, a multivariate error in variables model (EVM) technique (Patino Leal and Reilly, 1981) would be required to account for the effects of the many sources of error on rate parameter estimates. This type of systematic study has not yet been performed for the proprietary catalyst system under study.

Since rate constants have not been determined for the silica-supported magnesium and titanium-based industrial catalyst system used, initial order of magnitude estimates for rate constants were obtained from Kissin (1987) for similar catalyst systems. Propagation and transfer rate constants at individual sites were then manipulated to produce results corresponding to those determined experimentally by Usami et al. (1986). Two active site types were employed in the simulations. Rate constants were chosen such that site 1 produces higher molecular weight polymer, low in butene, and site 2 produces butene-rich, lower molecular weight polymer. Propagation rate constants were chosen so that the reactivity ratio product, r_1r_2, for site 1 was unity and r_1r_2 for site 2 was 0.55 as determined for a similar industrial catalyst by Usami et al. (1987). Transfer rate constants were manipulated in order to achieve weight average molecular weights corresponding to the melt index laboratory data and to achieve a polydispersity between 3.0 and 3.2 which is typical for the industrial catalyst used in the reactor.

Model predictions vs. plant data

Predictions were generated using the rate constants given in Table 1 and two industrial data sets as model input. While the constants from Table 1 give reasonable predictions of plant phenomena, they are not a unique set. Other combinations of constants can be developed to give identical predictions. From the simulations, it was determined that model predictions of production rate and copolymer composition were most sensitive to changes in the rate constants for propagation and copolymerization at the individual active site types. When CO was present in the reactor, impurity deactivation and desorption rate constants also became important. Molecular weight properties were influenced by the site-specific propagation, transfer to hydrogen and transfer to comonomer rate constants. Order of magnitude changes in the formation, initiation, transfer to cocatalyst, spontaneous transfer and spontaneous catalyst deactivation

Table 1. Rate Parameters for Model Predictions

		Site Type 1	Site Type 2
Formation, s^{-1}	$kf\ (j)$	1	1
Initiation, L/mol · s	$ki_1\ (j)$	1	1
	$ki_2\ (j)$	0.14	0.14
	$kh_1\ (j)$	1	1
	$kh_2\ (j)$	0.1	0.1
	$kh_r\ (j)$	20	20
Propagation, L/mol · s	$kp_{11}\ (j)$	85	85
	$kp_{12}\ (j)$	2	15
	$kp_{21}\ (j)$	64	64
	$kp_{22}\ (j)$	1.5	6.2
Transfer, L/mol · s	$kf_{11}\ (j)$	0.0021	0.0021
	$kf_{12}\ (j)$	0.006	0.11
	$kf_{21}\ (j)$	0.0021	0.001
	$kf_{22}\ (j)$	0.006	0.11
	$kfh_1\ (j)$	0.088	0.37
	$kfh_2\ (j)$	0.088	0.37
	$kfr_1\ (j)$	0.024	0.12
	$kfr_2\ (j)$	0.048	0.24
	$kfs_1\ (j)$	0.0001	0.0001
	$kfs_2\ (j)$	0.0001	0.0001
Deactivation, s^{-1}	$kds\ (j)$	0.0001	0.0001
L/mol · s	$kdI\ (j)$	2000	2000
Impurity Desorption, s^{-1}	$ka\ (j)$	0.0003	0.0003

reaction rate constants had very little influence on model predictions. A single set of rate constants were used to develop copolymer composition, molecular weight, and reaction rate predictions for both data sets. When a catalyst grade change was made, the numbers of active sites of each type per gram of catalyst were altered to reflect the hypothesis that each catalyst grade has a different distribution of the same two site types. The individual site 1 and site 2 rate constants, however, were not altered.

Data Set 1. In this period, the molecular weight remained relatively constant while a transition to a lower-density resin with a higher comonomer incorporation was performed. An interesting feature of this data set is that carbon monoxide was injected into the reactor and then the catalyst feed rate was interrupted. This data set represents 65 hours of continuous reactor operation. A single grade of catalyst was used throughout the operating period. Shown in Figure 4 is a comparison of the simulated rate of reaction and the overall rate of reaction as measured by an on-line heat balance. There is good qualitative agreement between the simulated and measured rates over the entire duration of the simulation. The marked drops in the reaction rate at 13 and 25 hours were caused by the presence of carbon monoxide in the reactor, followed by a catalyst feed disruption. Figure 5 is a plot of the CO concentration which was measured by an on-line gas chromatograph. Several simulations were run using different values of deactivation and reactivation rate constants $k_{dI}(j)$ and $k_a(j)$. Because of the nature of the catalyst feed rate shown in Figure 6, one cannot determine both the rates of desorption and subsequent reactivation of dead sites from this data set. Various combinations of k_{dI} and k_a gave similar reaction rate predictions. The results shown in Figure 4 were obtained using $k_{dI} = 2{,}000$ L/ mol · s and $k_a(j) = 0.0003$

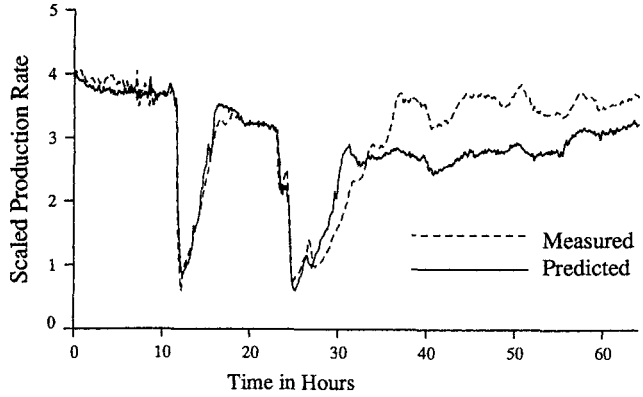

Figure 4. Comparison of predicted and measured production rates: data set 1.

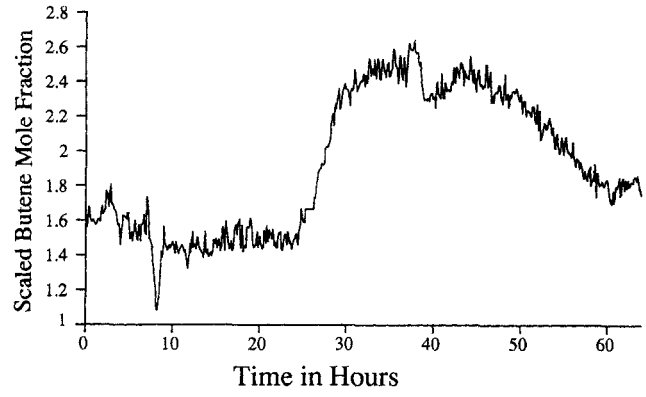

Figure 7. Scaled gas-phase butene concentration: data set 1.

L/ mol · s for both site types. For the first 25 hours, the predicted reaction rate is very similar to the rate estimated by the heat balance. After 28 hours, however, there is a quantitative mismatch between predicted and measured reaction rates. This discrepancy could not be alleviated by further tuning of the rate constants. Between 28 and 32 hours the measured rate is lower than the predicted rate. Thereafter, the measured rate remains higher than the prediction. The sustained mismatch in level after 32 hours may be due to several unmodeled phenomena. As shown in Figure 7 the level of butene in the reactor was significantly higher after 32 hours than during the first 25 hours. One would expect greater swelling of the amorphous regions of the polymer by butene during this period of high gas-phase butene concentrations. As discussed in Hutchinson and Ray (1988), the equilibrium sorption of both butene and ethylene are enhanced by this plasticizing effect, leading to higher polymerization rates than if the polymer were not swollen. The current model does not account for the swelling of the polymer by comonomer and thus, cannot predict rate increases due to this phenomenon. Other potential causes for the rate mismatch include batch to batch catalyst variability or a possible recalibration of the catalyst metering system. The presence of reactive feed impurities other than carbon monoxide may also have contributed to the rate mismatch.

A plot of the predicted active site distribution throughout the run is given in Figure 8. Since one grade of catalyst was used throughout the run and a negligible decay rate was assumed for both types sites, the ratio between the two site types remained constant throughout the simulation. Note that the introduction of CO into the cycle gas resulted in a marked decrease in number of active sites of each type. As shown in Figure 9, the molecular weight remained relatively constant throughout the run, except for a drop to 95 kg/mol between 30 and 35 hours. The model predicts the qualitative trend in the molecular weight, but there is a slight mismatch in level between 35 and 60 hours. This mismatch may also be due to the unmodeled

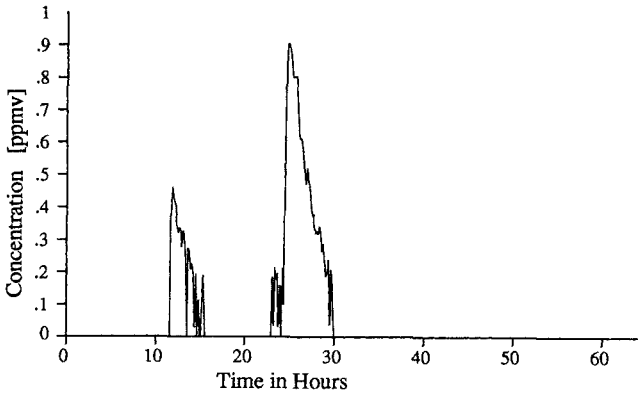

Figure 5. Carbon monoxide concentration in gas phase: data set 1.

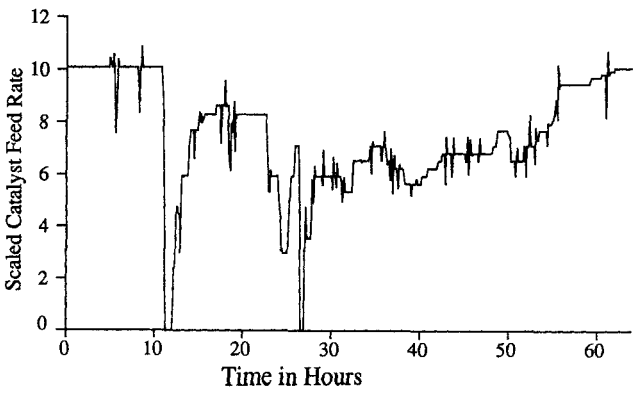

Figure 6. Catalyst feed rate to reactor: data set 1.

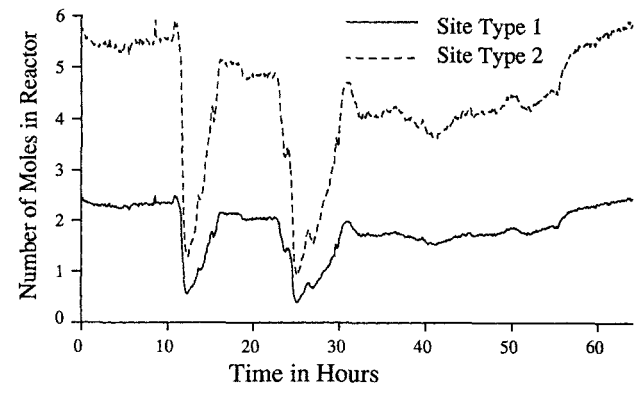

Figure 8. Number of moles of growing polymer chains at each site type: data set 1.

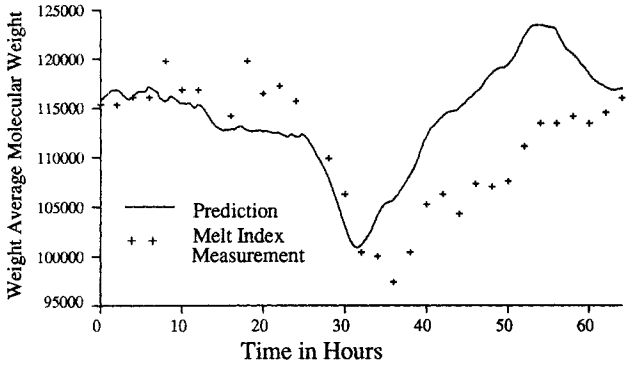

Figure 9. Predicted molecular weight vs. estimates from melt index laboratory data: data set 1.

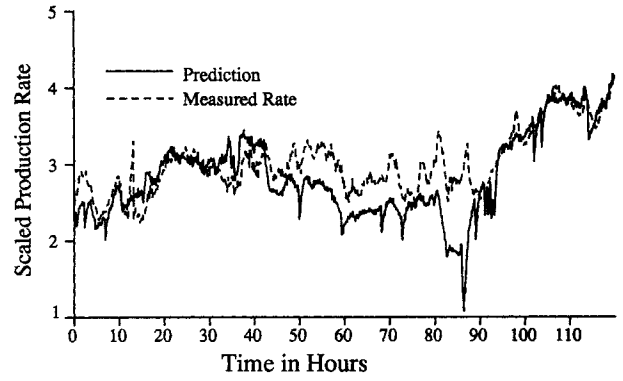

Figure 11. Comparison of predicted and measured production rates: data set 2.

solubility effects of the higher butene concentration. As illustrated in Figure 10, the comonomer incorporation predicted by the model corresponds nearly perfectly to the laboratory density measurements during the entire operating period.

Data Set 2. The second data set, which contains several molecular weight transitions, a transition in comonomer incorporation or density, and a catalyst grade change corresponds to 120 hours of continuous reactor operation. Illustrated in Figure 11 is a comparison of predicted and measured reaction rates. Both the detail and the overall level of the production rate is well predicted by the model except between 80 and 85 hours when a change in the catalyst grade occurs. A plot of the number of moles of active sites of each type is given in Figure 12. The catalyst grade change at 85 hours markedly changed the active site distribution. From the simulation results shown, it appears that the catalyst used to produce low molecular weight, high melt index material contained relatively more of active site 1 than did the catalysts used to produce high molecular weight, low melt index grades. Figure 13 is a comparison of weight average molecular weight predicted by the simulation and that determined from the laboratory melt index measurements. The comonomer incorporation predictions and estimates from laboratory density measurements are compared in Figure 14. The model was able to predict both molecular weight and copolymer composition very accurately throughout the entire operating period.

Molecular weight and copolymer composition distributions

From a comparison of the model predictions and the industrial production rate, *MI* and density data, it is apparent that the bulk properties of the polymer produced in the industrial reactor can largely be explained by the model. As well, the model can predict bimodal instantaneous molecular weight and composi-

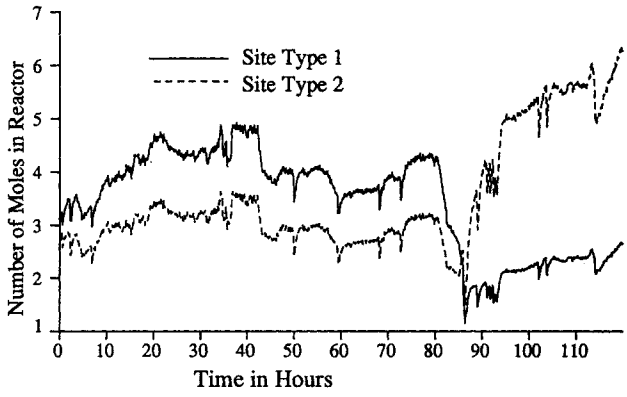

Figure 12. Number of moles of growing polymer chains at each site type: data set 2.

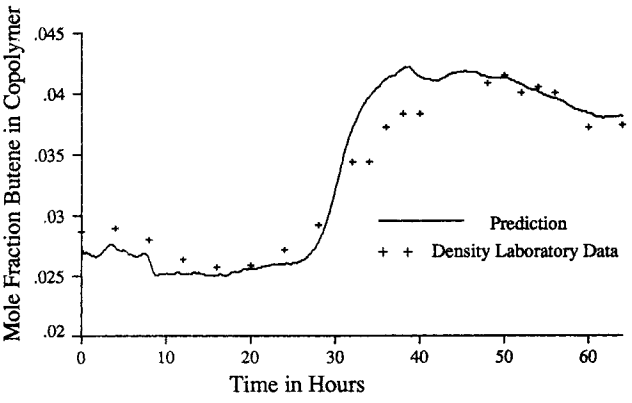

Figure 10. Predicted copolymer composition vs. estimates from density laboratory data: data set 1.

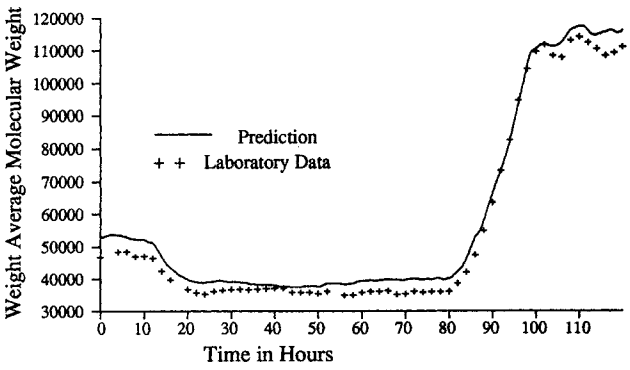

Figure 13. Predicted molecular weight vs. estimates from melt index laboratory data: data set 2.

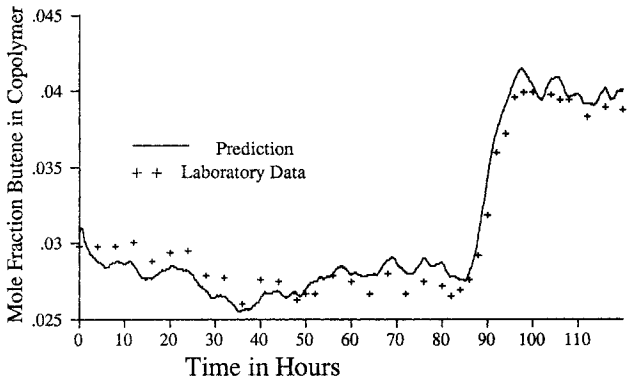

Figure 14. Predicted copolymer composition vs. estimates from density laboratory data: data set 2.

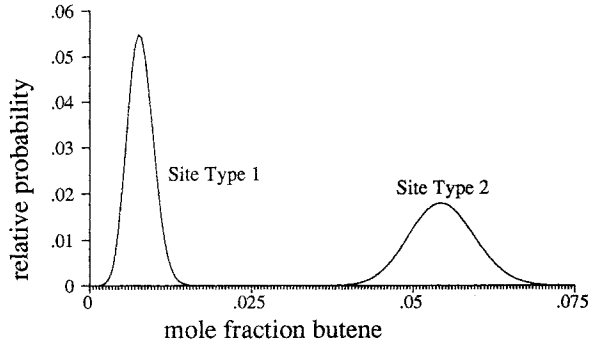

Figure 15. Instantaneous comonomer incorporation probability distribution function: data set 2.
Time = 10 hours

tional distributions which were observed by Usami et al. (1986) and Wild et al. (1982). Shown in Figures 15 and 16 are plots of instantaneous molecular weight and compositional distributions predicted from the model results for data set 2 at time 10 hours. This time was chosen because the reactor was operating at essentially steady state and, as such, the instantaneous properties correspond closely to bulk polymer properties in the reactor. Note that the polydispersity of the molecular weight distribution of the whole polymer is near 3.1, which is larger than 2.0, the

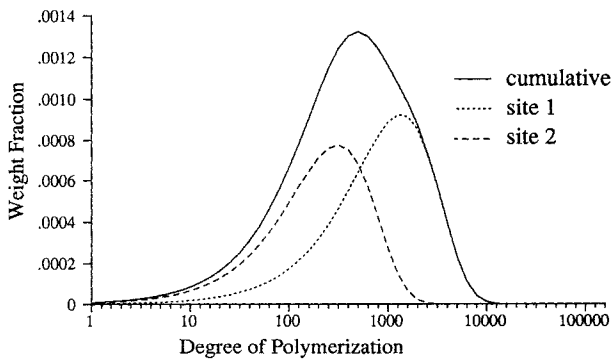

Figure 16. Instantaneous molecular weight distribution: data set 2.
Time = 10 hours

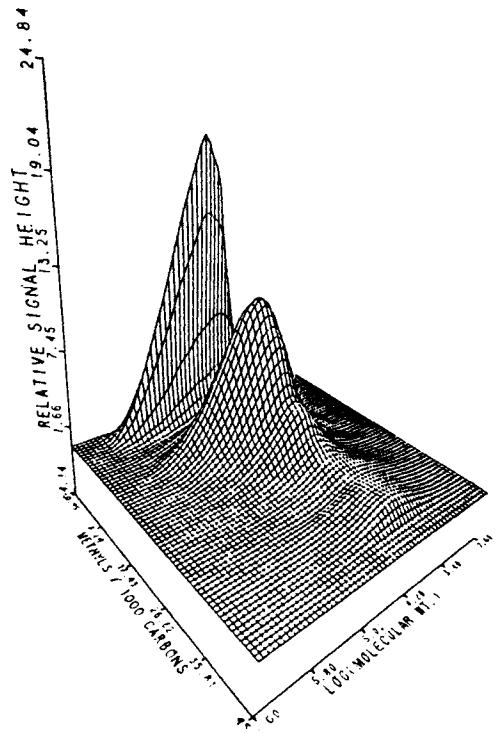

Figure 17. Experimental joint frequency distribution of molecular weight and short chain branching in a commercial linear low-density polyethylene sample.
Reproduced from Wild et al. (1982) with permission.

polydispersity of the polymer produced at each individual site type. The sites which produced the higher molecular weight polymer are responsible for the low butene peak in the compositional distribution. These results are very similar to Wild's experimental findings for a commercial polyethylene sample which are shown in Figure 17.

Conclusions

A dynamic kinetic model for the production of linear polyethylenes in a gas phase reactor has been presented. This model considers the existence of multiple types of active sites on the heterogeneous Ziegler-Natta catalyst. It has been shown that a two-site model can predict the changes in production rate, weight average molecular weight and copolymer composition which occur in response to gas phase composition and catalyst grade changes in an industrial reactor. As well, this model predicts a broadened molecular weight distribution and a bimodal copolymer compositional distribution which are typical of commercial linear polythylenes.

Acknowledgment

The authors thank the Natural Science and Engineering Research Council of Canada and ESSO Chemical Canada for support of this research.

Notation

$AlEt_3$ = triethyl aluminum cocatalyst
B_i = moles of reacted monomer of type i bound in the polymer in the reactor

F_i = mole fraction of the total polymer in the reactor which is composed of reacted monomer i

$\overline{F}_1(j)$ = Mean mole fraction ethylene in the polymer produced at sites of type j

f_i = fraction of total monomer in the reactant gas which is monomer M_i

$F^*_{in}(j)$ = molar flow rate of potential active sites of type j into the reactor

H_2 = hydrogen

I_m = impurity such as carbon monoxide

i = monomer type

j = active site type

$ka(j)$ = impurity desorption rate constant for a site of type j

$kdI(j)$ = deactivation by impurities rate constant for a site of type j

$kds(j)$ = spontaneous deactivation rate constant for a site of type j

$kf(j)$ = formation rate constant for a site of type j

$kfh_i(j)$ = transfer rate constant for a site of type j with terminal monomer M_i reacting with hydrogen

$kfm_{ik}(j)$ = transfer rate constant for a site of type j with terminal monomer M_i reacting with monomer M_k

$kfr_i(j)$ = transfer rate constant for a site of type j with terminal monomer M_i reacting with $AlEt_3$

$kfs_i(j)$ = spontaneous transfer rate constant for a site of type j with terminal monomer M_i

$kh_i(j)$ = rate constant for reinitiation of a site of type j by monomer M_i

$kh_r(j)$ = rate constant for reinitiation of a site of type j by cocatalyst

$ki_i(j)$ = rate constant for initiation of a site of type j by monomer M_i

K_p = partition coefficient between the gas and polymer phases

$kp_{ik}(j)$ = propagation rate constant for a site of type j with terminal monomer M_i reacting with monomer M_k

$\overline{m}$ = mean monomer molecular weight

M_1 = ethylene

M_2, M_3 = butene, hexene

M_c = critical molecular weight for application of power law relationship between viscosity and molecular weight

MI = melt index

M_i = monomer of type i

$\overline{M}_n$ = number average molecular weight of polymer

$\overline{M}_w$ = weight average molecular weight of polymer

mw_i = molecular weight of monomer M_i

$M_x(j)$ = instantaneous mass rate of polymer production at sites of type j

$N^*(j)$ = potential active site of type j

$N(0, j)$ = uninitiated site of type j produced by formation reaction

$N_d(j)$ = spontaneously deactivated site of type j

$Nd_I(0, j), Nd_{IH}(0, j)$ = impurity killed sites of type j

$N_H(0, j)$ = uninitiated site of type j produced by transfer to hydrogen reaction

$N_i(r, j)$ = living polymer molecule of length r, growing at an active site of type j, with terminal monomer M_i

NS = number of active site types

$Q(r, j)$ = dead polymer molecule of length r produced at a site of type j

r = number of units in polymer chain

r_1, r_2 = propagation reactivity ratio product

R_i = instantaneous consumption rate of monomer i

$R_i(j)$ = rate at which monomer i is consumed by propagation reactions at sites of type j

R_v = volumetric polymer phase outflow rate from the reactor

T = subscript referring to total of all monomer types

t = time

V_p = volume of polymer phase in the reactor

$W(r, y, j)drdy$ = weight fraction of instantaneous copolymer produced at a site of type j with chain length between r and $r + dr$ and composition between y and $y + dy$

$W(r, y)drdy$ = weight fraction of instantaneous copolymer produced at all sites with chain length between r and $r + dr$ and composition between y and $y + dy$

$Y(n, j)$ = nth moment of chain length distribution for living polymer produced at a site of type j

$X(n, j)$ = nth moment of chain length distribution for dead polymer produced at a site of type j

Z = polydispersity of molecular weight distribution

Greek letters

$\phi_i(j)$ = fraction of active sites of type j which have terminal monomer M_i

η = viscosity of polymer melt at low shear

κ = parameter in the Stockmayer bivariate distribution

ρ = polymer density

$\sigma(j)^2$ = standard deviation of the copolymer compositional distribution at site type j

$\tau(j)$ = ratio of the total rate of transfer to the total rate of propagation at sites of type j

Literature Cited

Boehm, L. L., J. Berthold, R. Franke, W. Strobel, and U. Wolfmeier, "Ziegler Polymerization of Ethylene: Catalyst Design and Molecular Weight Distribution," *Stud. Surf. Sci. Cat.*, **25**, 29 (1986).

Burdett, I. D., "The Union Carbide UNIPOL Process: Polymerization of Olefins in a Gas-Phase Fluidized Bed," AIChE Meeting, Washington DC (Nov., 1988).

Choi, K. Y., and W. H. Ray, "Recent Developments in Transition Metal Catalyzed Olefin Polymerization—A Survey: 1. Ethylene Polymerization," *JMS-Rev. Macromol. Chem. Phys.*, **C25**(1), 1 (1985).

deCarvalho, A. B., P. E. Gloor, and A. E. Hamielec, "A Kinetic Mathematical Model for Heterogenous Ziegler-Natta Copolymerization," *Polym.* **30**, 280 (1989).

Floyd, S., K. Y. Choi, T. W. Taylor, and W. H. Ray, "Polymerization of Olefins through Heterogeneous Catalysis: III. Polymer Particle Modelling with an Analysis of Intraparticle Heat and Mass Transfer Effects," *J. Appl. Polym. Sci.*, **32**, 2935 (1986).

Floyd, S., T. Heiskanen, and W. H. Ray, "Solid Catalyzed Olefin Polymerization," *Chem. Eng. Prog.*, **84**(11), 56 (1988).

Galvan, R. "Modelling of Heterogeneous Ziegler-Natta Copolymerization of α-olefins," PhD Thesis, Univ. Minnesota (1986).

Galvan, R., and M. Tirrell, "Molecular Weight Distribution Predictions for Heterogeneous Ziegler-Natta Polymerization Using a Two-Site Model," *Chem. Eng. Sci.*, **41**, 2385 (1986).

Hamielec, A. E., J. F. MacGregor, and A. Penlidis, "Multicomponent Free-Radical Polymerization in Batch, Semi-Batch and Continuous Reactors," *Makromol. Chem., Macromol. Symp.*, **10/11**, 521 (1987).

Hindmarsh, A. C., "LSODE and LSODI, Two New Initial Value Ordinary Differential Equation Solvers," *ACM-Signum Newslett.*, **15**(4), 10 (1980).

Hutchinson, R. A., and W. H. Ray, "Polymerization of Olefins through Heterogeneous Catalysis: VII. Particle Ignition and Extinction Phenomena," *J. Appl. Polym. Sci.*, **34**(2), 657 (1987).

———, "Sorption Effects in Heterogeneous Catalyzed Olefin Polymerization," AIChE Meeting, Washington DC (Nov. 28, 1988).

Kissin, Y. V., *Isospecific Polymerization of Olefins with Heterogeneous Ziegler-Natta Catalysts*, Springer-Verlag, New York (1987).

Kunii, D., and O. Levenspiel, "Bubbling Bed Model for Kinetic Processes in Fluidized Beds. Gas—Solid Mass and Heat Transfer and

Catalytic Reactions," *I&EC Process Design and Dev.*, 7(4), 481 (1968).
Levenspiel, O., *Chemical Reaction Engineering*, 2nd ed., Wiley, Toronto, 2nd ed., 144 (1972).
Nagel, E. J., V. A. Kirrillov, and W. H. Ray, "Prediction of Molecular Weight Distributions for High Density Polyolefins," *Ind. Eng. Chem. Prod. Res. Dev.*, **19**, 372 (1980).
Patino Leal, H., and P. M. Reilly, "A Bayesian Study of the Error-in-Variables Model," *Technometrics*, **23**, 221 (1981).
Sinclair, K. B., "Characteristics of Linear LPPE and Description of UCC Gas Phase Process," Process Economics Report, SRI International, Menlo Park, CA (1983).
Stockmayer, W. H., "Distribution of Chain Lengths and Composition in Copolymers," *J. Chem. Phys.*, **13**, 199 (1945).
Tacx, J. C. J. F, H. N. Linssen, and A. L. German, "Effect of the Molar Mass Ratio of Monomers on the Mass Distribution of Chain Lengths and Compositions in Copolymers: Extension of the Stockmayer Theory," *J. Polym. Sci., Polym. Chem.*, **26**, 61 (1988).
Usami, T., Y. Gotoh, and S. Takayama, "Generation Mechanism of Short-Chain Branching Distribution in Linear Low-Density Polyethylenes," *Makromolec.*, **19**(11), 2722 (1986).
Vinogradov, G. V., and A. Ya. Malkin, *Rheology of Polymers—Viscoelasticity and Flow of Polymers*, Mir Publishers, Moscow, Chap. 2, 153 (1980).
Wild, L., T. R. Ryle, and D. C. Knobeloch, "Branching Distributions in Linear Low-Density Polyethylenes," *Polym. Prepr., (Amer. Chem. Soc. Div. Polym. Chem.)*, **23**(2), 133 (1982).
Zucchini, U., and G. Cecchin, "Control of Molecular Weight Distributions in Polyolefins Synthesized with Ziegler-Natta Catalytic Systems," *Adv. in Polym. Sci. Ind. Dev.*, **51**, 101 (1983).

Manuscript received Sept. 27, 1989, and revision received Mar. 8, 1990.